Retarded modes of a lateral antiferromagnetic/nonmagnetic superlattice

Xuan-Zhang Wang
Chinese Center of Advanced Science and Technology (World Laboratory), P.O. Box 8730, Beijing 10080, Peoples Republic of China and Department of Physics, Harbin Normal University, Harbin 150080, People's Republic of China

D. R. Tilley
School of Physics, Universiti Sains Malaysia, 11800 USM Penang, Malaysia and Department of Physics, University of Essex, Colchester CO4 3SQ United Kingdom

(Received 8 May 1995)

Using the effective-medium theory, we investigate the surface polaritons of a lateral antiferromagnetic nonmagnetic superlattice in the Voigt geometry and obtain some interesting analytical results. Calculation dispersion curves for a FeF_2/ZnF_2 superlattice show differences in dispersion properties from a pure semi-infinite antiferromagnet and common antiferromagnetic nonmagnetic superlattice. (i) For $H_0=0$, the surface mode only exists in the condition $1 \geqslant f_1 \geqslant 0.5$ (f_1 is the antiferromagnetic fraction and H_0 indicates the field) and when $f_1 \neq 1.0$, the surface mode no longer starts from the boundary of the corresponding bulk continuum. For $f_1 = < 0.5$ no virtual surface mode is found. (ii) For $H_0 \neq 0$, three surface-polariton modes are obtained and one of them partly enters the bulk continuum. As $f_1 < 0.5$ only two surface modes can exist. They are virtual and in the bulk continuum. The computed attenuated total reflectivity is also presented.

I. INTRODUCTION

In recent years, the application of molecular-beam epitaxy to the fabrication of high-quality ultrathin magnetic films and superlattices has made it possible to study various novel properties in superlattices with different structures. A semi-infinite lateral superlattice has a surface perpendicular to the interface between the two different constituent layers.[1] However, a lateral superlattice film has two surfaces of this kind.[2] This superlattice or superlattice film can be fabricated by using a combination of electron- and ion-beam lithography.[3–5] In previous papers,[1,2] we dealt with ferromagnets and studied the surface magnetostatic modes in a lateral semi-infinite superlattice and the surface magnetostatic modes and magnetostatic guided modes of a lateral superlattice film. For numerical calculations, we took the Ni/Mo system as an example and obtained some interesting numerical results, besides the analytic results.

In this paper we consider a semi-infinite antiferromagnetic/nonmagnetic superlattice with a lateral surface normal to the layers (LANS), as shown in Fig. 1. We restrict our attention to the situation where the magnetic field applied in the direction of the easy axis is small so that the sublattice magnetization stays in the direction of the axis, which is parallel to the layers and surface. We assume the period of the LANS is short enough that it can be described as a single effective medium, which means

$$kL \ll 1, \tag{1}$$

where k is the magnitude of the wave vector and $L=L_1+L_2$ the period of the superlattice. The inequality (1) implies that the propagation is near the center of the superlattice minizone $0<k<\pi/L$) so that effects related to the magnetic gaps at the minizone boundaries $k=\pm n\pi/L$ are not important.

Our aim is to determine the general characteristics of the surface mode in the LANS and to compare them with those in pure antiferromagnets[6,7] and ordinary antiferromagnetic/nonmagnetic superlattices.[8,9]

As defined in Fig. 1, L_1 and L_2 are the thicknesses of the antiferromagnetic layers and nonmagnetic layers, respectively. We introduce $f_1=L_1/L$ and $f_2=L_2/L$, called the magnetic and nonmagnetic fractions, respectively, so that $f_1+f_2=1$.

II. DISPERSION EQUATION OF THE EFFECTIVE MEDIUM

As shown by Fig. 1, the coordinate system is such that the z axis is the uniaxis, with the y axis normal to the surface, and the wave vector k is directed along the x axis. The magnetic field (H_0) and magnetization (M_0) of the sublattices are in the direction of the z axis.

In the absence of damping, the permeability tensor of the

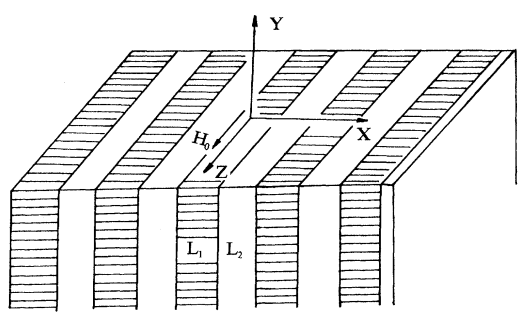

FIG. 1. Illustration of lateral antiferromagnetic/nonmagnetic superlattice. L_1 and L_2 are the thicknesses of the antiferromagnetic layers and nonmagnetic layers, respectively. H_0 represents an external magnetic field and the magnetizations are in the direction of the z axis. The propagation of the wave is along the x axis.

0163-1829/95/52(18)/13353(5)/$06.00

antiferromagnetic layers can be written as

$$\mu_1=\begin{pmatrix} \mu & i\mu_\perp & 0 \\ -i\mu_\perp & \mu & 0 \\ 0 & 0 & 1 \end{pmatrix}, \tag{2}$$

where the expressions of μ and $\mu_\perp$ are

$$\mu=1+\omega_a\omega_m\{[\omega_r^2-(\omega_0-\omega)^2]^{-1}+[\omega_r^2-(\omega_0+\omega)^2]^{-1}\}, \tag{3}$$

$$\mu_\perp=\omega_a\omega_m\{[\omega_r^2-(\omega_0-\omega)^2]^{-1}-[\omega_r^2-(\omega_0+\omega)^2]^{-1}\}, \tag{4}$$

with

$$\omega_m=4\pi\gamma M_0, \tag{5}$$

$$\omega_a=\gamma H_a, \tag{6}$$

$$\omega_0=\gamma H_0, \tag{7}$$

$$\omega_r=\gamma\sqrt{2H_aH_e+H_a^2}. \tag{8}$$

In these expressions, H_a represents the anisotropy field, H_e the exchange field, and γ the gyromagnetic ratio. M_0 is the sublattice magnetization. ϵ_1 is the dielectric constant of the layers.

For the nonmagnetic layers, the permeability $\mu_2=1$ and we write ϵ_2 for their dielectric constant. With the effective-medium theory, the magnetic permeability of the LANS, described as a single effective medium, can be written as[10,11]

$$\mu^e=\begin{pmatrix} \mu_{xx} & i\mu_{xy} & 0 \\ -i\mu_{xy} & \mu_{yy} & 0 \\ 0 & 0 & 1 \end{pmatrix} \tag{9}$$

with

$$\mu_{xx}=(f_1/\mu+f_2), \tag{10a}$$

$$\mu_{xy}=f_1\mu_\perp/(f_1+f_2\mu), \tag{10b}$$

$$\mu_{yy}=f_1\mu+f_2-f_1f_2\mu_\perp^2/(f_1+f_2\mu). \tag{10c}$$

At the same time, the effective dielectric constant is expressed by

$$\epsilon=f_1\epsilon_1+f_2\epsilon_2. \tag{11}$$

Following the method used in Ref. 12, the Maxwell's equations, satisfied by the surface wave in the form $\exp(ikx-i\omega t)$ and decaying exponentially with distance from the surface, result in

$$\epsilon\omega^2(\mu_{xx}\mu_{yy}-\mu_{xy}^2)+(\alpha^2\mu_{yy}-\mu_{xx}k^2)=0, \tag{12}$$

where the decay factor α within the medium is real and positive.

The boundary conditions produce

$$\alpha\mu_{yy}+\alpha_0(\mu_{xx}\mu_{yy}-\mu_{xy}^2)-ku_{xy}=0, \tag{13}$$

$$\alpha_0=\sqrt{k^2-\omega^2}. \tag{14}$$

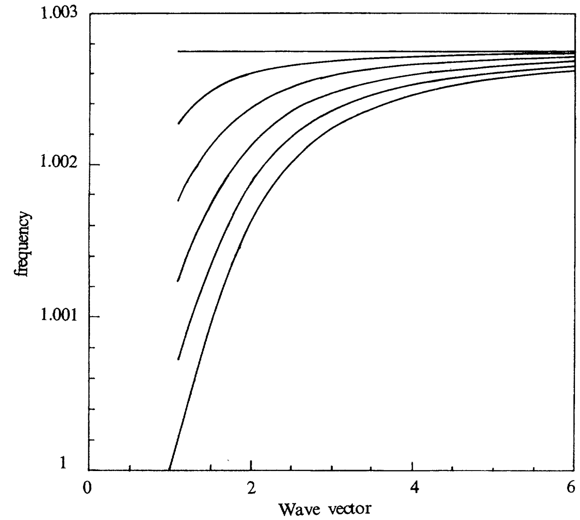

FIG. 2. Dispersion curves of surface-retarded modes for $H_0=0$. The curves from the top to the bottom are related to $f_1=0.5$, 0.6, 0.7, 0.8, 0.9, and 1.0, respectively. The frequency and wave vector are quoted in ω_r.

In (12) and (13), we have taken the light velocity $c=1$. Utilizing (13) to eliminate α in (12), one can determine the dispersion relation explicitly. Alternatively, one can use (12) and (13) to compute the dispersion curves directly. To see the physics, we start with a simple case, $H_0=0$. Because $\mu_{xy}=0$ in this case, (12) and (13) can be reduced to

$$\epsilon\omega^2\mu_{xx}\mu_{yy}+\alpha^2\mu_{yy}-k^2\mu_{xx}=0, \tag{15}$$

$$\alpha+\alpha_0\mu_{xx}=0. \tag{16}$$

We easily find that (15) and (16) result in a very simple dispersion relation:

$$\epsilon\omega^2\mu_{yy}+(k^2-\omega^2)\mu_{xx}\mu_{yy}-k^2=0 \tag{17}$$

with the additional conditions $k^2>\omega^2$, $\mu_{xx}<0$ to ensure $a_0>0$, and $a>0$. Some further interesting relations for the existence of the surface mode may be obtained. First we change Eq. (17) into

$$\omega^2/k^2=(\mu_{yy}^{-1}-\mu_{xx})/(\epsilon-\mu_{xx}), \tag{18}$$

which implies

$$0\leqslant(\mu_{yy}^{-1}-\mu_{xx})/(\epsilon-\mu_{xx})\leqslant 1. \tag{19}$$

Combining (19) with the condition $\mu_{xx}<0$, we have the frequency window of the surface mode,

$$\omega_r^2+2f_2\omega_m\omega_a<\omega^2<\omega_s^2, \tag{20}$$

where

$$\omega_s^2=\omega_r^2+\omega_m\omega_a. \tag{21}$$

Equation (20) also shows that, in the case of $H_0=0$, the surface mode only exists in the range $1\geqslant f_1\geqslant 0.5$ and that the magnetostatic limit ω_s does not change with f_1. Unlike the superlattice[8] with the surface parallel to the magnetic layers, for $H_0=0$ here virtual surface modes cannot exist. In addi-

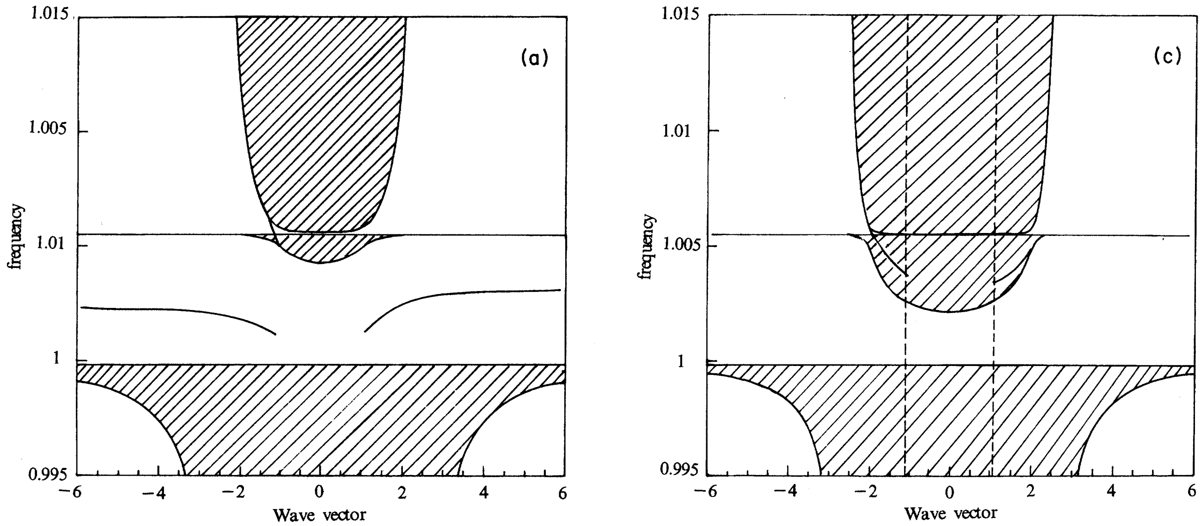

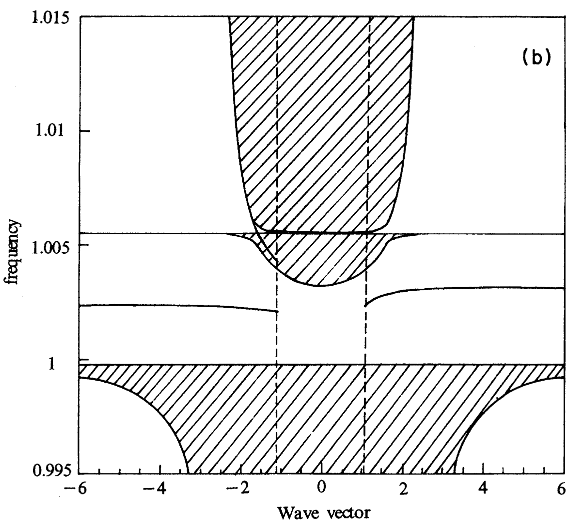

FIG. 3. Dispersion curves of surface-retarded modes for $H_0=0.2$ kG. (a) $f_1=0.8$, (b) $f_1=0.6$, and (c) $f_1=0.4$. The frequency and wave vector are quoted in ω. In (b) and (c) ATR scan lines are included for later comparison with Fig. 5.

tion, an increase in frequency of the bottom limit of the window with f_2 can cause the separation of the surface-mode branch from the bulk continuum. This point is different qualitatively from the corresponding bulk system and superlattices like that in Ref. 8. For the superlattice of Ref. 8, one can obtain the two frequency windows of the surface mode for $f_1<0.5$ and $f_1>0.5$, in the form $\omega_r^2<\omega^2<\omega_r^2+2f_1\omega_m\omega_a$ and $\omega_r^2<\omega^2<\omega_r^2+\omega_m\omega_a$. The first window determines the existence of the virtual surface mode.

Since we are not able to find an explicit equation for ω from (12) and (13), or from (18) in the case of $H_0=0$, numerical calculations for dispersion curves are necessary. Examples of the dispersion curves are computed for a lateral FeF_2/ZnF_2 superlattice in the fields $H_0=0$ and 0.2 kG. We take the parameters as follows: $M_0=0.56$ kG, $H_a=200$ kG, $H_e=540$ kG, $\gamma=1.97\times10^7$ rad/G, and $\epsilon_1=5.5$ for the antiferromagnetic layers; $\epsilon_2=8.0$ and $\mu_2=1.0$ for the nonmagnetic layers.

First we consider the case of $H_0=0$, in which the propagation is reciprocal, $\omega(k)=\omega(-k)$. Figure 2 presents several typical examples of the dispersion curves for different values of the magnetic fraction f_1. We find that the surface mode only exists for $f_1>0.5$ and has the same magnetostatic limit ω_s for all f_1. As f_1 is decreased from 1, the starting point of the mode on the vacuum light line rises so that the mode separates from the bulk continuum. However, for a pure antiferromagnet or an ordinary antiferromagnetic/nonmagnetic superlattice, the surface mode always start at the upper boundary ($\omega=\omega_r$) of the lower bulk continuum. Also, unlike the situation for the ordinary superlattice,[8] here there are not any virtual modes.

Generally speaking, in contrast to the situation for $H_0=0$, the three bulk continua and the surface-mode propagation are not reciprocal for a bulk antiferromagnet in a field.[6] For our LANS the striking effects of a modest applied field $H_0=0.2$ kG are illustrated by Fig. 3. For the magnetic fraction $f_1>0.5$ three surface-mode branches can appear; the two lower surface-mode branches have a magnetostatic limit and are real. However it is very interesting that as seen in Figs. 3(a) and 3(b) the upper mode partly enters the middle bulk continuum and becomes a kind of mode similar to what one can see in surface phonon polaritons.[14] When $f_1<0.5$ the $-k$ lower surface mode disappears and the $+k$ one

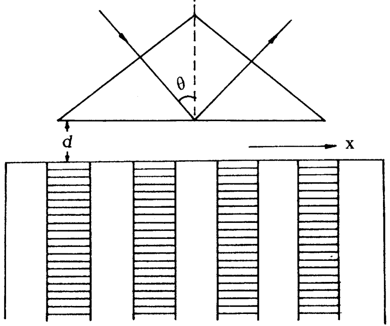

FIG. 4. Geometry for the ATR calculation, θ is the incident angle.

moves entirely into the middle bulk continuum, as seen in Fig. 3(c). This kind of magnetic surface mode is rare. Another feature is that as the magnetic fraction f_1 is lowered the upper surface mode on the $-k$ side becomes obvious, which is contrary to the property of the corresponding surface mode in the superlattice with a surface parallel to the layers.[12]

III. ATTENUATED TOTAL REFLECTION SPECTRA

Attenuated total reflection (ATR) spectroscopy has proved effective in investigating surface modes.[6,12,13] In Fig. 4 we show the geometry with incident light at an angle θ to the y axis in a prism of dielectric constant ϵ_p. θ is larger than the critical angle $\theta_c=\sin(1/\epsilon_p)$. The prism and superlattice are separated by a vacuum spacer of thickness d. In our geometry the in-plane wave vector is in the direction of the x axis and

$$k'_x=k=\epsilon_p^{1/2}(\omega/c)\sin\theta, \tag{22}$$

$$k'_y=\epsilon_p^{1/2}(\omega/c)\cos\theta. \tag{23}$$

When we calculate ATR spectra, it is necessary to include a damping term in μ and $\mu_\perp$, so that ω in (3) and (4) is replaced by $\omega+i\Gamma$.

The expression for ATR reflectivity can easily be obtained with the method given in Ref. 6 and here it is

$$R=(A-1)/(A+1) \tag{24}$$

with

$$A=ik'_y[F+\exp(2\alpha_0 d)]/\{[\alpha_0(F-\exp(2\alpha_0 d)]\}. \tag{25}$$

Using (14), F is simply expressed as

$$F=[\alpha_0(\mu_{xx}\mu_{yy}-\mu_{xy}^2)+\mu_{xy}k-\alpha\mu_{yy}]/[\alpha_0(\mu_{xx}\mu_{yy}-\mu_{xy}^2)+\mu_{yy}\alpha-\mu_{xy}k)], \tag{26}$$

where α and α_0 are determined by (12) and (14), respectively. The interesting reflected ATR is $|R|^2$.

For numerical calculations we take a Si prism ($\epsilon_p=11.6$ and $\theta_c=17.1°$) with a gap $d=0.03$ cm and damping $\Gamma=10$ G. Computed ATR reflectivities in a field of $H_0=0.2$ kG are shown in Figs. 5 for $f_1=0.6$ and 0.4; the corresponding dispersion curves are shown in Figs. 3(b) and 3(c).

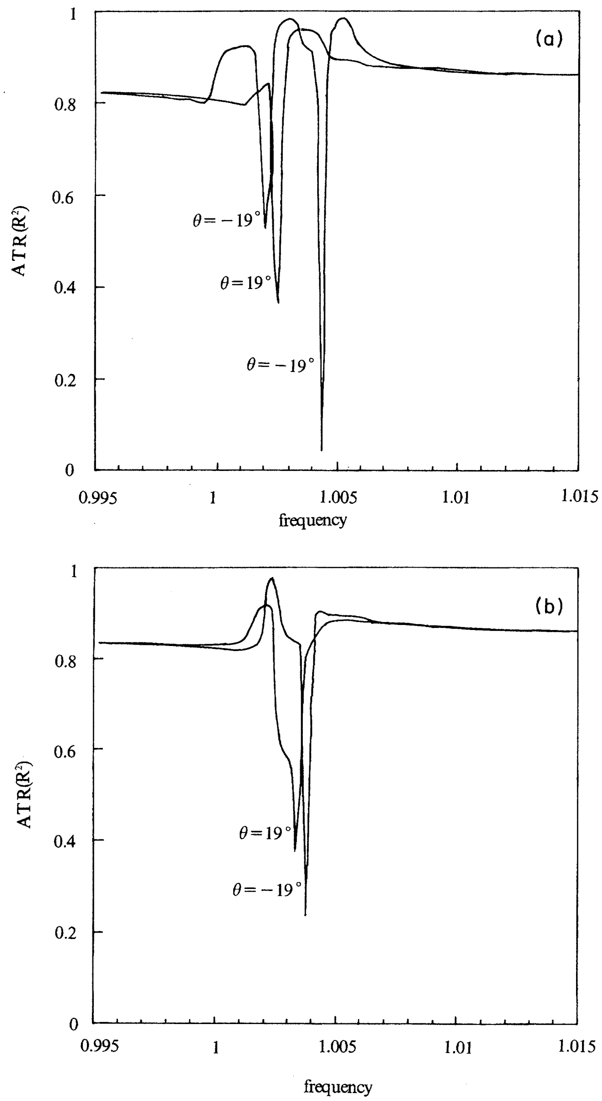

FIG. 5. Attenuated total reflectivity as a function of frequency for H_0=0.2 kG, $\theta=\pm19°$, and d=0.03 cm. (a) f_1=0.6 and (b) f_1=0.4. The frequency is quoted in ω_r.

The ATR frequency scan at fixed angle is along the line in the ω-k plane given by (22). Because of the very fine frequency scale in Fig. 3, this is accurately represented by $k=1.1$ in the units of that figure. The corresponding scan lines for $+\theta$ and $-\theta$ are shown in Figs. 3(b) and 3(c). In practice it is the direction of the applied field H_0 rather than θ that would be reversed but the effect is the same. The rules for qualitative interpretation of an ATR spectrum are these. Where the scan line is in a bulk continuum, $|R|^2<1$ because some power is transmitted into bulk modes. Between bulk continua, that is, a stop band for the bulk modes, $|R|^2\approx1$ since no power can be transmitted. However, where the scan line intersects a surface-polariton line a dip in $|R|^2$ is seen because power can couple into the surface polariton. It can be seen that Figs. 5(a) and 5(b) are indeed "mappings" of Figs. 3(b) and 3(c) in this sense. For example, the $\theta=-19°$ curve in Fig. 5(a) starts at a low frequency and with $|R|^2<1$ because the scan line [Fig. 3(b)] is in the lower bulk continuum. The spectrum then rises towards unity as the scan line enters the lower stop band, but then dips sharply at the first surface mode. The dip corresponding to the second surface mode appears within the region $|R|^2<1$ of the second bulk continuum. $|R|^2$ then rises to near 1 at the position of the narrow higher stop band before falling again to $|R|^2<1$ in the highest bulk continuum.

We remark finally that simple oblique-incidence reflectivity can be a very effective probe of antiferromagnetic resonance lines.[15,16] Calculation of such spectra is a very straightforward matter, given the form of μ, and we have chosen not to present results of this kind.

IV. CONCLUSION

We have studied the surface modes for the lateral antiferromagnetic/nonmagnetic superlattice, and the computed dispersion curves and attenuated total reflectivities are consistent. Our results apply for $kL \ll 1$ where the LANS can be considered as a single effective medium. Comparing the results in this paper with those for the pure antiferromagnet[6] and antiferromagnetic/nonmagnetic superlattice with the surface parallel to the layers (ANS),[12] one can find some interesting differences. First, unlike ANS's and the pure antiferromagnet, for $1>f_1>0.5$ and field $H_0=0$, the surface mode is isolated, or is completely separated from the bulk continuum; for $f_1<0.5$, no virtual surface mode (without magnetostatic limit) is found. Second, for $H_0\neq 0$ and $f_1<1$, the surface mode can partly enter the middle bulk continuum. In particular, for $f_1<0.5$, only two surface modes are seen, and they are virtual and in the middle bulk continuum.

We believe that the calculations presented here are timely in that techniques are already available for the sample preparation and the measurements. Epitaxial superlattices of antiferromagnetic FeF_2 and CoF_2,[17] CoO/NiO,[18–20] and Fe_3O_4/NiO (Refs. 21–23) have been successfully prepared and their properties studied. Clearly, the preparation of epitaxial angle films by these techniques is possible. Processing into a LSL structure is then a lithographic problem.[3–5] The final question concerns feasibility of ATR measurements. As is to be expected for antiferromagnets, the frequency scales in Figs. 3 and 5 are very fine. For FeF_2, with a resonance frequency of about 50 cm^{-1}, the full horizontal scale in Fig. 5 runs from 49.75 to 50. 75 cm^{-1}. Fourier-transform spectra of bulk FeF_2 with a resolution of 0.06 cm^{-1} have been published[15,16] and a resolution of 0.02 cm^{-1} is available. We therefore believe that measurement of spectra on the frequency scale of Fig. 5 is practical.

ACKNOWLEDGMENTS

X.-Z.W. thanks the Science Foundation of Heilongjiang Province for financial support.

[1] Xuan-Zhang Wang and D. R. Tilley, Phys. Lett. A **187**, 325 (1994).
[2] Xuan-Zhang Wang and D. R. Tilley, Phys. Rev. B **50**, 13 472 (1994).
[3] C. Shearwood, S. J. Blundell, M. J. Baird, J. A. C. Bland, M. Gester, H. Ahmed, and H. P. Hughes (unpublished).
[4] Y. Ueska, Y. Nakatini, and N. Hayashi, J. Magn. Magn. Mater. **123**, 209 (1993).
[5] C. Shearwood, H. Ahmed, L. M. Nicolson, J. A. C. Bland, M. J. Baird, M. Patel, and H. P. Hughes, Microelectron. Eng. **21**, 431 (1993).
[6] R. E. Camley and D. L. Mills, Phys. Rev. B **26**, 1280 (1982).
[7] S. Cao and A. Caille, Solid State Commun. **42**, 233 (1982).
[8] N. S. Almeida and D. R. Tilley, Solid State Commun. **73**, 23 (1990).
[9] J. Barnas, J. Phys. Condens. Matter **2**, 7173 (1990).
[10] N. Raj and D. R. Tilley, Phys. Rev. B **36**, 7003 (1987).
[11] N. S. Almeida and D. L. Mills, Phys. Rev. B **38**, 6698 (1988).
[12] M. C. Oliveros, N. S. Almeida, D. R. Tilley, J. Thomas, and R. E. Camley, J. Phys. Condens. Matter **4**, 8497 (1992).
[13] M. G. Cottam and D. R. Tilley, *Introduction to Surface and Superlattice Excitations* (Cambridge University Press, Cambridge, England, 1989).
[14] D. N. Mirlin, in *Surface Polaritons*, edited by V. M. Agranovich and D. L. Mills (North-Holland, Amsterdam, 1982).
[15] D. E. Brown, T. Dumelow, T. J. Parker, Kamsul Abraha, and D. R. Tilley, Phys. Rev. B **49**, 12 266 (1994).
[16] Kamsul Abraha, D. E. Brown, T. Dumelow, T. J. Parker, and D. R. Tilley, Phys. Rev. B **50**, 6808 (1994).
[17] C. A. Ramos, D. Lederman, A. R. King, and V. Jaccarino, Phys. Rev. Lett. **65**, 2913 (1990).
[18] M. Takano, T. Torashima, Y. Bando, and H. Ikida, Appl. Phys. Lett. **51**, 205 (1987).
[19] J. A. Borchers, M. J. Carey, R. W. Erwin, C. F. Majkzak, and A. E. Berkowitz, Phys. Rev. Lett. **70**, 1878 (1993).
[20] M. J. Carey, A. E. Berkowitz, J. A. Borchers, and R. W. Erwin, Phys. Rev. B **47**, 9952 (1993).
[21] D. M. Lind, S. D. Borry, G. Chern, H. Mathias, and L. R. Testardi, Phys. Rev. B **45**, 1838 (1992).
[22] D. M. Lind, S. P. Tay, S. D. Berry, J. A. Borchers, and R. W. Erwin, J. Appl. Phys. **73**, 6886 (1993).
[23] J. A. Borchers, R. W. Erwin, S. D. Berry, D. M. Lind, E. Lochner, and K. A. Shaw, Appl. Phys. Lett. **64**, 381 (1994).